Article

Economic and Environmental Multi-objective Optimization of a Wind-Solar-Fuel Cell Hybrid Energy System in the Colombian Caribbean Region

Guillermo Valencia [1], Aldair Benavides [1] and Yulineth Cárdenas [2,*]

[1] Departamento de Ingeniería Mecánica, Universidad del Atlántico, Carrera 30 Número 8-49, Puerto Colombia, Área Metropolitana de Barranquilla 080007, Colombia; guillermoevalencia@mail.uniatlantico.edu.co (G.V.); aebenavides@mail.uniatlantico.edu.co (A.B.)

[2] Departamento de Energía, Universidad de la Costa, Barranquilla 080002, Colombia; ycardena6@cuc.edu.co

* Correspondence: ycardena6@cuc.edu.co; Tel.: +575-324-94-31

† These authors contributed equally to this work.

Abstract: The hybrid system is analyzed and optimized to produce electric energy in Non-Interconnected Zones in the Colombian Caribbean region, contributing both to the improvement in the reduction of greenhouse gas emissions and to the rational use of energy. A comparative analysis of the performance of these systems was carried using a dynamic model in real wind and solar data. The model is integrated by a Southwest Wind Power Inc. wind turbine. AIR 403, a proton exchange fuel cell (PEM), an electrolyze, a solar panel and a charge regulator based on PID controllers to manipulate oxygen and hydrogen flows in the cell. The transient responses of the cell voltage, current, and power were obtained for the demand of 200 W for changes in solar radiation and wind speed for all days of the year 2013 in the Ernesto Cortissoz airport, Puerto Bolívar, Alfonso Lopez airport and Simon Bolívar airport, by regulating the flow of hydrogen and oxygen into the fuel cell. The maximum contribution of power generation from the fuel cell was presented for the Simon Bolívar airport in November with a value of 158,358W (9.45%). A multi-objective design optimization under a Pareto front is presented for each place studied to minimize the Levelized Cost of Energy and CO_2 emission, where the objective variables are the number of panel and stack in the PV system and PEM.

Keywords: Fuel cell; wind energy, solar energy, hybrid energy system; Colombian caribbean region; multi-objective optimization.

1. Introduction

In response to the global problem of greenhouse gas emissions and global warming, many countries have begun to diversify their energy matrix by incorporating renewable energy generation systems [1]–[4]. The potential growth of these generation systems has allowed this solution has positioned as a mature technology in the energy sector [5]–[7], significantly impacting on the improvement of energy and environmental indicators in some nations [8].

In Colombia, national regulations have motivated the rational use of energy and preservation of the environment [9], emphasizing renewable resource generation systems such as solar and wind energy [10]–[12]. However, currently the percentage contribution of these systems is low compared to conventional generation systems, the main source being hydroelectric with 69,5%, followed by thermal with 29,6% and renewable with a percentage less than 1% (0,9%) [13], which corresponds to the few investigations developed to evaluate the energy performance of hybrid power generation

Peer-reviewed version available at Energies 2019, 12, 2119; doi:10.3390/en12112119

systems, when they operate with the energy resources available in the different regions of the country [14], [15]. Since hybrid power generation systems allow switching the energy source to meet demand, these have been extensively studied when proposing energy solutions in areas not interconnected to the grid [13] [16]–[18].

Simulations of this type of the system had been developed on both small and large scale [19]. In addition to experimental studies [20], even taking into account the tidal energy source with highly sophisticated and robust mathematical formulations [21]. On the other hand, in countries such as Brazil, photovoltaic solar technology has been integrated into hybrid systems [22], since it is a highly reliable and functional energy alternative [23], with advantages such as the use of few parts, low maintenance requirements and quiet operation [24], [25]. Even in Mexico, the study of this system in the Veracruz region was being highlighted [26].

The main contribution of this study is to evaluate the complementarity of wind, solar and electric power generation in a proton-exchange fuel cell (PEM), through a dynamic model of a hybrid system operating in different places in the Colombian Caribbean Region for the demand of 200W. A multi-objective optimization under a Pareto front is presented for each place studied to minimize the Levelized Cost of Energy and CO_2 emission.

2. Methodology

2.1. Description of the region and information

The Colombian Caribbean region, as shown in Figure 1, is located in the north of the country with a population of approximately 11 million people, located in the area of roughly 132.270,5 km^2 (11,6% of the national territory) [27]. It is bounded to the north by the Atlantic Ocean, to the east by Venezuela, to the west by the Pacific Ocean and the south by the Andean region, is made up from flat areas except Magdalena and the snow-capped mountains (5.755 m) and a full coastal region. Also with a climatic diversity ranging from tropical to subtropical, where the average temperature is 30°C and even reaching up to 35°C in the Riohacha because of its arid and desert zone.

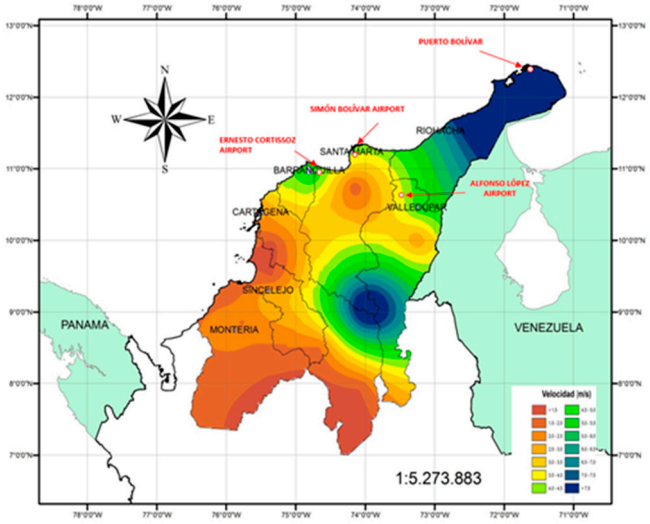

Figure 1. Geographical location of the places studied in the Caribbean region (Colombia).

2.2. System description

The hybrid energy power generation system (HEPGS) as shown in Figure 2 is integrated by a solar power generation module, with a unit power ratio of 37,08 W, a maximum voltage and current of 16,56 V and 2,25 A respectively, for a total of 36 cells in series and 1 in parallel [28], a Southwest Wind Power Inc. wind turbine AIR 403 with the ability to generate a peak power of 820 W at a wind

Peer-reviewed version available at Energies 2019, 12, 2119; doi:10.3390/en12112119

speed of 40 miles/hour [28], and a PEM fuel cell, which produces 401,23 W, a voltage and current of 48 V and 8,26 A, when a molar flow of hydrogen and the oxygen of 0,005 mol/s at 25°C supplied to the chemical reaction. The system was complemented with an electrolyzer for the generation of hydrogen and power regulator that operates with two PID controllers tuned to the Ziegler Nichols method to manipulate the flow of oxygen and the hydrogen that has been supplied to the cell [29].

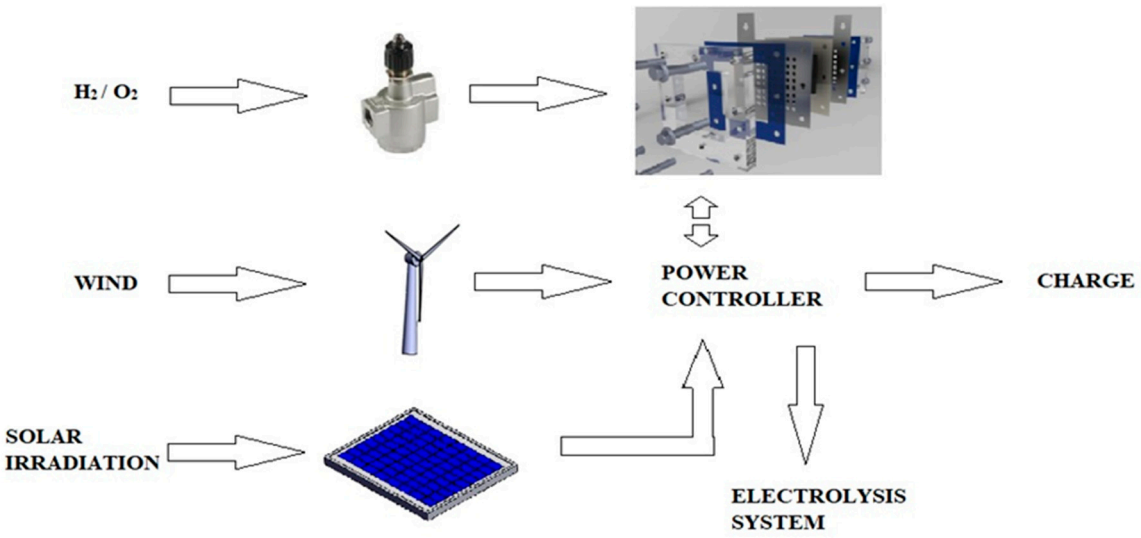

Figure 2. Hybrid power generation system schematic diagram.

2.3. Dynamic fuel cell model

The dynamics of the PEM type fuel cell has been extensively studied [30], where the thermodynamic potential E is calculated using the Nernst Equation [31], resulting in the Equation 1

$$E = 1.229 - 0.85 \times 10^{-3}(T - 298.1) + 4.3085 \times 10^{-5}\left(\ln p_{h_2} + 0.5 \ln p_{o_2}\right) \quad (1)$$

The concentration of dissolved oxygen in the gas/liquid interface is defined by Henry's law, as shown in Equation 2

$$Co_2 = \frac{p_{o_2}}{5.8 \times 10^{-6} \exp\left(\frac{-498}{T}\right)} \quad (2)$$

Excess stress due to activation and internal resistance is calculated by Equations 3 and 4, which are experimental relationships

$$n_{act} = 0.00312T - 0.86514 - 0.000187 \ln(i) + 7.4 \times 10^{-5} T \ln Co_2 \quad (3)$$

$$R_{int} = 0.01605 - 3.5 \times 10^{-5} T + 8 \times 10^{-5} I \quad (4)$$

Fuel cell current and activation resistance are related as

$$R_a = -\frac{n_{act}}{i} \quad (5)$$

The output voltage of the fuel cell is given by Equation 6

$$V = E + \eta_{ohmic} - V_{act} \quad (6)$$

The dynamics of the activation voltage of the fuel cell is described by Equation 7

$$\frac{dV_{act}}{dt} = \frac{i}{c} - \frac{cV_{act}}{R_a} \quad (7)$$

The loss of the ohmic voltage and the total voltage contained in the fuel cell is described by Equations 8 and 9 respectively

$$\eta_{ohmic} = -iR_{int} \quad (8)$$

$$V_{stack} = 65V_{cell} \quad (9)$$

Anode and cathode pressure are calculated as shown in Equations 10 and 11

$$\frac{V_a}{RT}\frac{dp_{H_2}}{dt} = \dot{m}_{H_2-in} - \left(\rho_{H_2} U A_r\right)_{out} - \frac{1}{2F} \quad (10)$$

$$\frac{V_a}{RT}\frac{dp_{O_2}}{dt} = \dot{m}_{O_2-in} - \left(\rho_{O_2} U A_r\right)_{out} - \frac{1}{4F} \quad (11)$$

The energy balance in the air-cooled fuel cell was expressed by Equation 12

$$\frac{dT}{dt} = 65i^2\frac{(R_a + R_{int})}{C_{ht}} - \frac{C_{ht}(T - T_r)}{R_t} \quad (12)$$

The rate of hydrogen production in the electrolyzer is given by Faraday's Law as shown in Equation 13

$$n_{H_2} = \frac{n_F n_C i_e}{2F} \quad (13)$$

Finally, the relationship between the theoretical and actual maximum amount of hydrogen produced by the electrolyze is given by Equation 14

$$n_F = 96.5\exp\left(\frac{0.09}{i_e} - \frac{75.5}{i^2_e}\right) \quad (14)$$

2.4. Dynamic model of the photovoltaic solar panel

The model used for the photovoltaic solar system is described by Equations 15 and 19, with parameters and operational values available in modeling studies of hybrid systems [32]–[34], where the panel current is given by Equation 15 [28]

$$I_{ph} = [I_{SCr} + K_i(T - 298)] \times 0.001\lambda \quad (15)$$

In the same way, the inverse saturation current is defined. ($\boldsymbol{I_{rs}}$) and the saturation current ($\boldsymbol{I_o}$), which is dependent on the temperature of the panel, are given by the Equations 16 y 17 respectively

$$I_{rs} = \frac{I_{SCr}}{\left[\exp\left(\frac{qVoc}{N_s kAT}\right) - 1\right]} \quad (16)$$

$$I_o = I_{rs}\left(T/T_r\right)^3 \exp\left[\left(\frac{qE_{go}}{Bk}\right)\left(\frac{1}{T_r} - \frac{1}{T}\right)\right] \quad (17)$$

The output current of the cell corresponds to Equation 18

Preprints (www.preprints.org) | NOT PEER-REVIEWED | Posted: 19 April 2019 doi:10.20944/preprints201904.0221.v1

Peer-reviewed version available at Energies 2019, 12, 2119; doi:10.3390/en12112119

$$I_{PV} = N_p \times I_{ph} - N_p \times I_o \left[\exp\left(\frac{q \times (V_{pv} + I_{PV} R_s)}{N_s A K T} \right) - 1 \right] \quad (18)$$

where $V_{pv} = V_{OC,} N_p = 1\ y\ N_s = 36$. Finally, the total power is given by Equation 19

$$P_{PV} = V_{PV} \times I_{PV} \quad (19)$$

The performance of the photovoltaic cell is related to the solar irradiation available at the site of operation of the system, which for this study was based on the year 2013 [35], resulting in the behavior shown in Figure 3

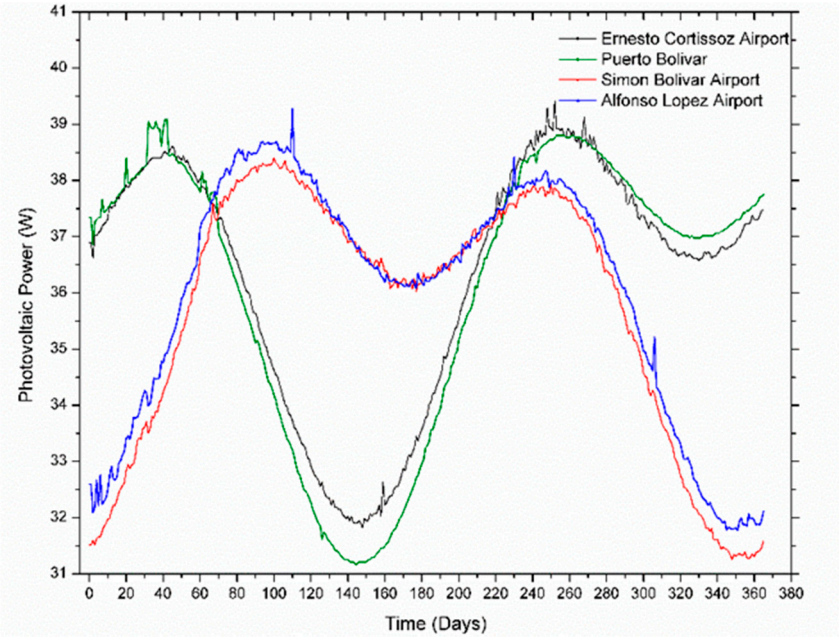

Figure 3. Photovoltaic power response for Ernesto Cortissoz, Puerto Bolívar, Simon Bolívar and Alfonso Lopez.

The similarity in the behavior of the power generated by the PV, at the Ernesto Cortissoz airport and Puerto Bolívar, is due to the irradiation, which is similar in both places. In the same way, the behavior for the other two energy substations is correlated to the same effect. The dimensioning of the PV system was given in order to meet the consumption of the processing unit of a weather station to be installed in the Colombian Caribbean region.

2.5. Dynamic model of the wind power

The third source of energy presented in the hybrid system was wind energy, which is a function of wind speed at the operating height of the wind turbine. For the projection of wind speed at axle height, Hellmann's law was applied [36] as is shown in the Equation 20

$$\frac{v}{v_o} = \left(\frac{h}{h_o} \right)^{\propto} \quad (20)$$

where $\boldsymbol{v}$ is the wind speed at height h to be calculated, $\boldsymbol{v_o}$ is the wind speed at a reference height $\boldsymbol{h_o}$ and $\propto$ is the wind velocity at the altitude of is the relative roughness, values available for these places in the wind Atlas [36].

The dynamic behavior of the power generated by the wind turbine operating in each of the study sites is shown in Figure 4.

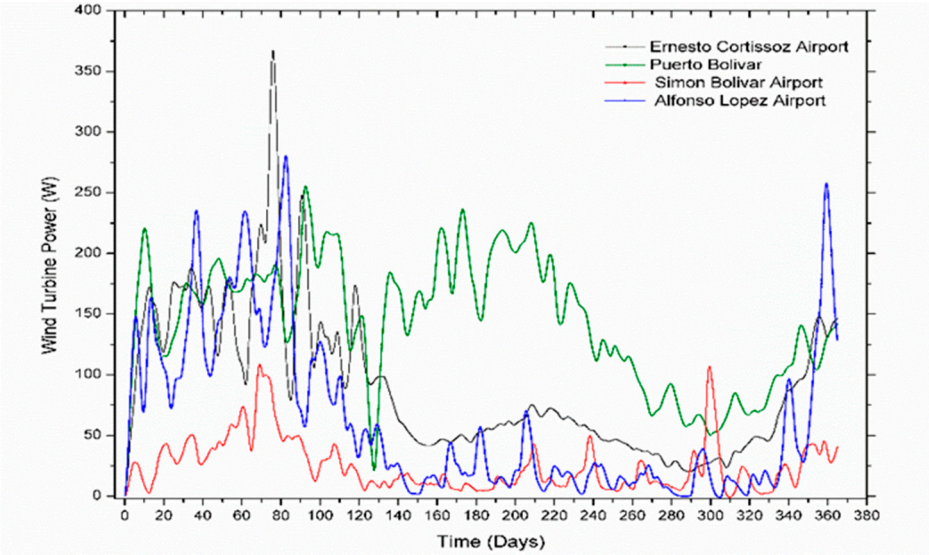

Figure 4. Dynamic behavior of wind power through a complete year at 100 meters high.

3. Results

3.1. Results of dynamic behavior

Under the dynamic conditions established by the HEPGS in the different places of interest, the complementarity of solar and wind energy with the energy delivered by the PEM cell was evaluated to supply the 200W demand. To achieve the desired power in the cell, the molar flow of oxygen and hydrogen was regulated by PID controllers, obtaining the flow behavior shown in Figure 5 and Figure 6. For the case of Ernesto Cortissoz airport as shown in Figure five, during January to August the cell operated at a low loading rate with the molar flow for hydrogen and oxygen of 7.50e-05 mol/s for both because wind power generation along with solar energy supplied 67.7% of the total energy generated. However, from September to December, the flows had a variation between 0.0005 to 0.0045 mol/s which meant a contribution of 53.45% cell equivalent to 427.61W in the year.

For the case of the Puerto Bolívar station, both the molar flow of hydrogen and oxygen that entered the PEM cell presented a constant behavior throughout the year with a value of 0,000075 mol/s as shown in the Figure 5 due to the significant amount of wind energy generated, presenting a total of 2159.26W (81,168%) of total wind and solar power generation and for the cell a total of 484.32W (18,32%) for the whole year 2013.

As to the behavior of the system operating at Simon Bolívar airport, during the period from January to March. The cell, produced with a low molar flow regime of both hydrogen and oxygen with a value of 0,0075 mol/s, reaching the generation of wind and solar energy 40% of the total energy generated, while in early April to December, the PEM-type cell required the maximum molar flow of hydrogen and oxygen with a value of 0,0035 mol/s and 0,0017 mol/s respectively, generating a total of 1314.69 W (73,03%).

Finally, the operation of the system at Alfonso Lopez airport, led to the cell having a low charge generation between January and early August, with a value of 7.50e-05 mol/s for the input of hydrogen and oxygen flow, thus giving a combined production between solar and wind power of 58,41%, while for molar flow of oxygen presented the first change on Saturday August 3 with a value of 0,0017 mol/s and hydrogen for Friday, August 9th with a value of 0,00119 mol/s as shown in Figure 6, which was associated to the significant change in meteorological conditions, caused by a decrease in wind speed in the place so that the generation of the wind and solar component of the system

Preprints (www.preprints.org) | NOT PEER-REVIEWED | Posted: 19 April 2019 doi:10.20944/preprints201904.0221.v1

Peer-reviewed version available at Energies 2019, 12, 2119; doi:10.3390/en12112119

decreased so that the PEM started to generate energy to supply the demand. In order, to provide the energy demand at critical operational points, the cell reached the molar flow values of hydrogen and maximum oxygen at the beginning of August and December, with values of 0,0035 mol/s and 0,0017 mol/s respectively, operational points that represented an energy generation of 1015.78 W (66,84%).

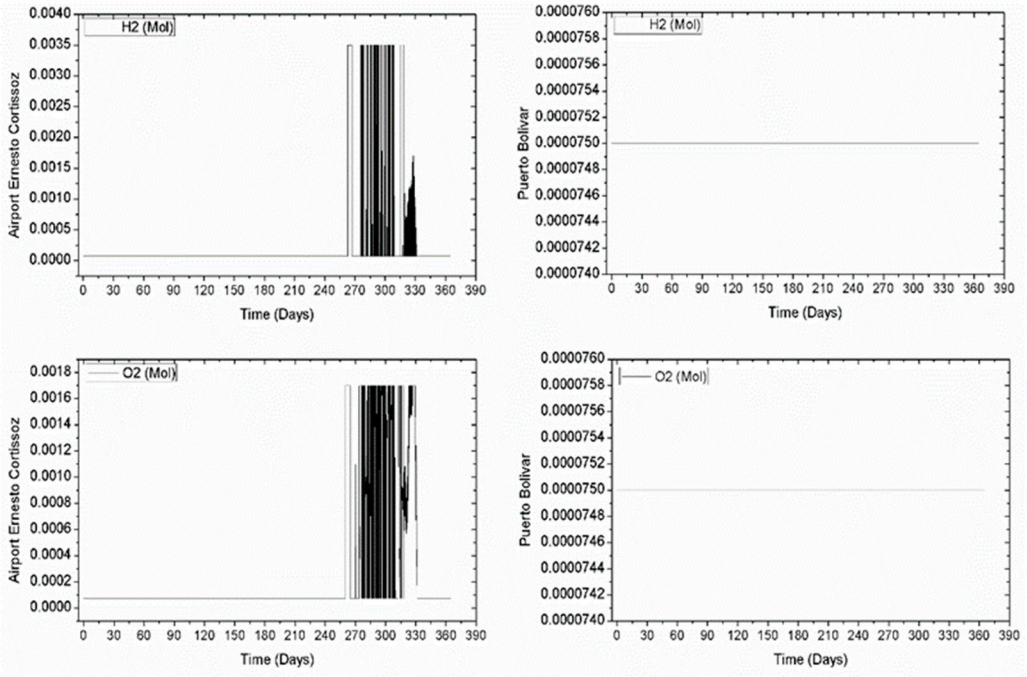

Figure 5. Hydrogen and molecular oxygen at the entrance to Ernesto Cortissoz airport and Puerto Bolívar.

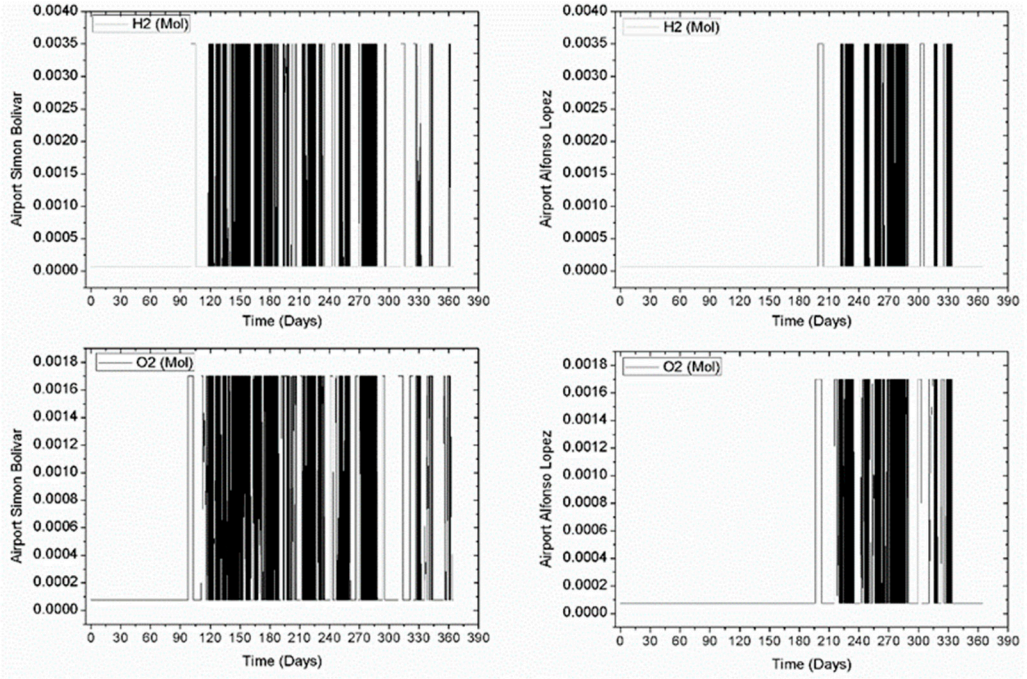

Figure 6. Hydrogen and molecular oxygen at the entrance to Simon Bolívar and Alfonso Lopez airport.

The variations in the voltage and electrical current in the cell for the places studied are shown in Figure 7, where it is highlighted that the maximum value of the current was presented for Alfonso Lopez Airport with an amount of 3,97A at the end of May because at this time the speed of viewing was about 85% below its average value. On the other hand, the maximum voltage was not presented in the same place, but at Ernesto Cortissoz airport with a value of 61,8V for January 16, values that

were the result of a cell power of 12,675W, which is a low contribution of this component (1,13%) compared to the other days of January, where the cell reached percentage peaks of generation on January 1 and 2 with values of 144,62W and 123,79W respectively.

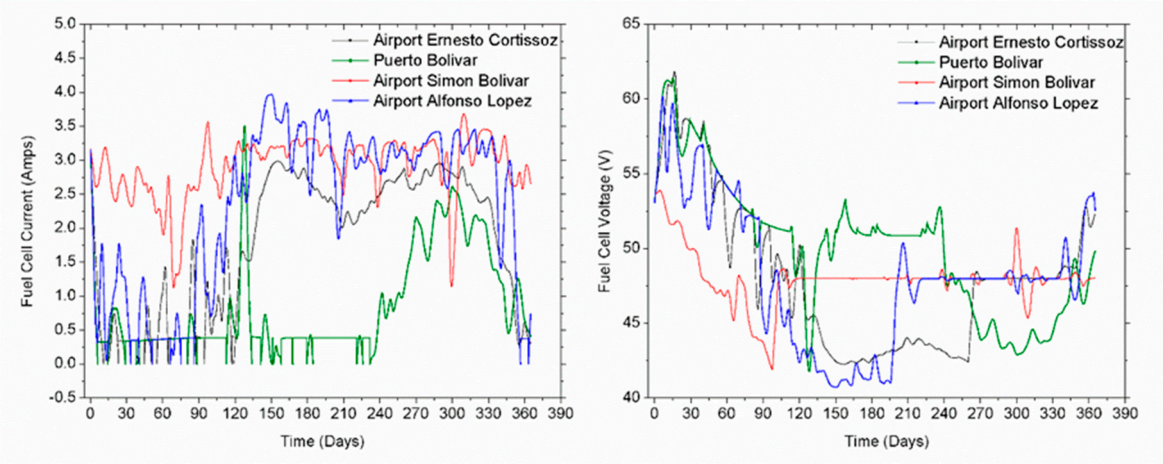

Figure 7. Fuel cell electrical voltage and current at Ernesto Cortissoz, Puerto Bolívar, Simon Bolívar and Alfonso Lopez.

The dynamics of the power of the PEM type fuel cell, operates in cases of low electricity generation using wind and solar resources to reach the demand of 200W. The power generation of the fuel cell was found by obtaining voltage and current from Figure seven for each of the energy substations studied as shown in the figure 8.

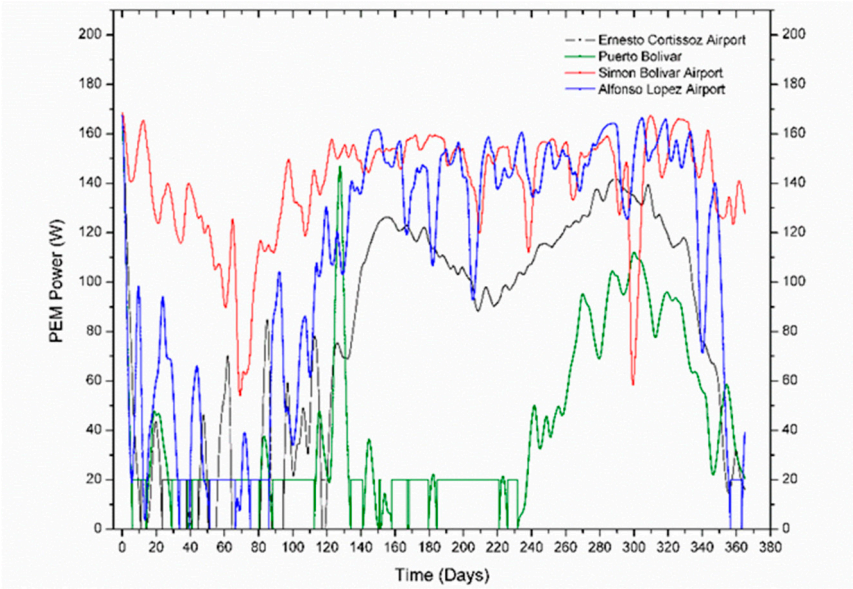

Figure 8. Fuel cell electrical voltage and current at Ernesto Cortissoz, Puerto Bolívar, Simon Bolívar and Alfonso Lopez.

For the demand of 200W, the respective values for each energy source were obtained, allowing the complementarity of these energy alternatives to be evaluated in each station, where similar behavior is highlighted for the power generated by the photovoltaic solar panel in all the study sites. Additionally, it was determined that the PEM-type cell produced more energy in September for the Simon Bolívar airport with a monthly power of 158,358W (9,45%), while the lower value was presented in Puerto Bolívar with 18,141W (3,745%) as shown in Figure 9, in which in the same way it can be observed that in some months the established demand is surpassed, due to the fact that the

Preprints (www.preprints.org) | NOT PEER-REVIEWED | Posted: 19 April 2019 doi:10.20944/preprints201904.0221.v1

Peer-reviewed version available at Energies 2019, 12, 2119; doi:10.3390/en12112119

energetic resource is fluctuating because of the given meteorological conditions, even the cell cannot stop working, that is why in the places where there are high values of wind and solar energy the demand is surpassed, which implies the storage of this one in a bank of condensers.

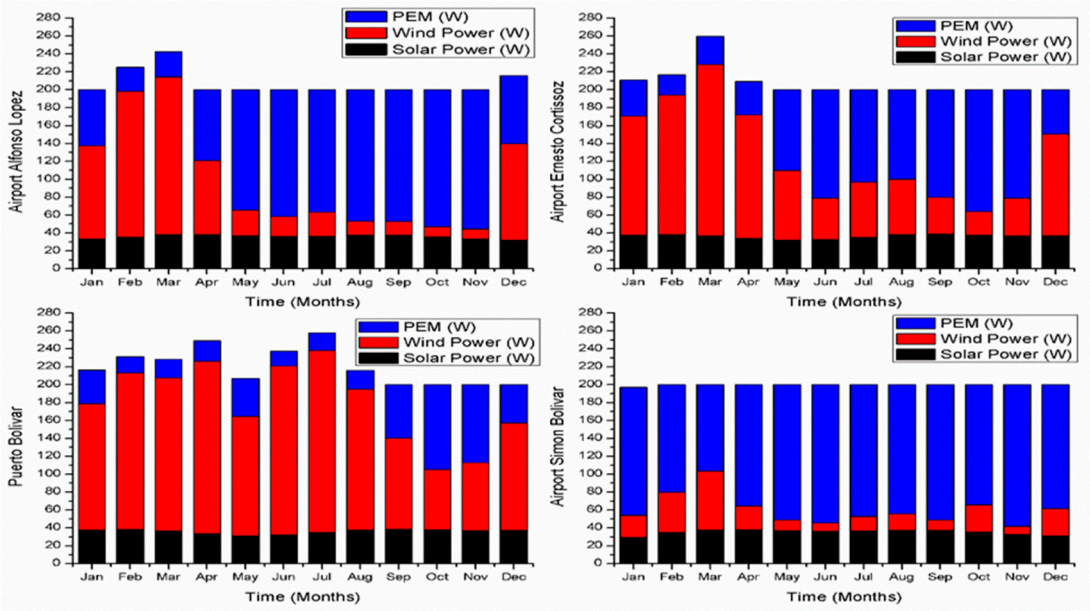

Figure 9. Accumulated power from different energy sources for different substations.

3.2. *Multi-objective optimization*

An optimization problem searches for the optimal value of a target function, which corresponds to a minimum or maximum of the function. However, in many engineering applications complex designs are required that lead to a simultaneous optimization of multiple functions which results in a conflict between objectives, which will make the improvement of one place to a worsening of the other. For this reason, the technique generates a matrix of decision variables with the possible optimal values of the problem. Equation 21 represents the mathematical expression of multi-objective optimization subject to the restriction of each of the functions and the range of evolution of the decision variables

$$\min F(X) = [f_1(X), f_2(X), f_3(X) \dots, f_n(X)]^T \quad (21)$$

Subject to, $g_i(X) \leq 0, \quad i = 1, \dots, m$

$h_i(X) \leq 0, \quad j = 1, \dots, n$

$X_{k,min} \leq X_k \leq X_{k,max}$,

where X denotes the vector of the decision variables to be optimized, $F(X)$ is the vector of the objective function, $g_i(X)$ are the inequality constraints, $h_i(X)$ are the equality constraints, $X_{k,min}$ and $X_{k,max}$ are lower and upper limits of the decision variables, respectively.

For this case, the genetic algorithm of non-dominated classification (NSGA-II) [37]-[38], combined with the programming code of the model was used to optimize the objectives developed in this study.

The systems used for each site introduce the optimization of two objective functions in which the cost per kWh of energy generated and the amount of CO_2 emissions per year are minimized, calculated using Equations 22 and 23, respectively

$$f_1(X) = LCE = \frac{\frac{i(1+i)^{T_s}}{(1+i)^{T_s}-1}C_{tot} + COM}{(E_{net})t_{op}} \quad (22)$$

$$f_2(X) = e_{CO_2} = e_{CO_2/sol} * P_{PV} + e_{CO_2/wind} * E_{wind} + e_{CO_2/O_2} * n_{O_2} + e_{CO_2/H_2} * n_{H_2} \quad (23)$$

The objective functions are evaluated with respect to the parameters of the designed model, in order to select the decision variables of the genetic algorithm. Likewise, the range of values that can be taken by each optimization criterion is determined, which are considered as design restrictions for each of the cases. Table 1 shows the selected decision variables with the minimum and maximum values it takes during the parametric study and the multi-objective optimization.

Table 1. Decision variables on the multi-objective optimization.

Decision variables	Symbol	Maximum value	Minimum value	Criteria
Number of panels	N_p	36	180	C1
Number of stacks	N_s	63	67	C2

In this section, a parametric evaluation is performed on the system to calculate the effect of the variation of the selected decision variables on the target functions for each of the locations under study. Figure 10 shows the variations of the LCE and the amount of CO_2 emissions with the increase of the decision criteria.

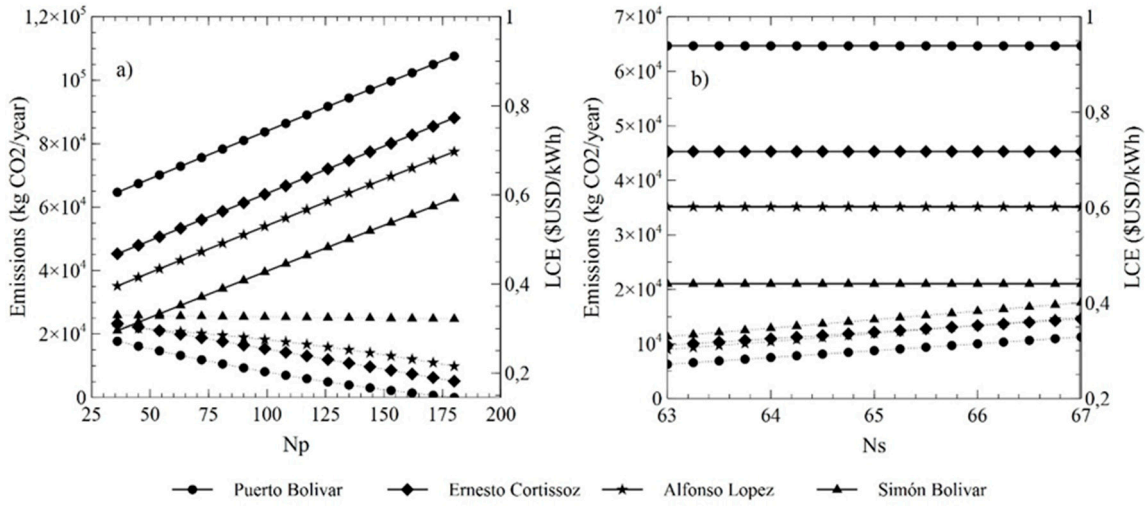

Figure 10. Variations of the LCE and CO_2 emissions with the decision criteria; a) Number of panels, b) Number of stacks.

Figure 10 shows that despite the different locations being studied, variations in target functions have the same trend for both cases, both in the increase in the number of panels and in the increase in the number of stacks. The increase in the number of installed panels increases the CO_2 emissions in the system, on the other hand, there is a decrease in costs per kWh due to the increase in energy generation capacity (Figure 10a).

The increase in the number of stacks generates an increase in LCE but in turn does not infer the amount of CO_2 emissions (Figure 10b). The location that presents the highest LCE values is Simon Bolívar, for this reason, the use of the minimum number of stacks installed in the system is considered.

This study shows that the town of Puerto Bolivar is the site with the highest amount of CO_2 emissions per year, thus being a determining factor in optimization.

In this case, 25 installation configurations were available for each of the power generation systems located in the airports of Puerto Bolívar, Ernesto Cortissoz, Alfonso Lopez and Simon Bolívar; with 453 possible iterations inside the generic algorithm. During optimization in each of the locations, a population of 100 values was generated for each of the decision variables in the ranges determined, as well as these were taken to calculate the objective functions in each of the points. And thus 35 possible solutions of the objective functions are obtained. Figure 11 shows the Pareto frontiers for the LCE with the CO_2 emissions and three possible optimal points, in each of the locations.

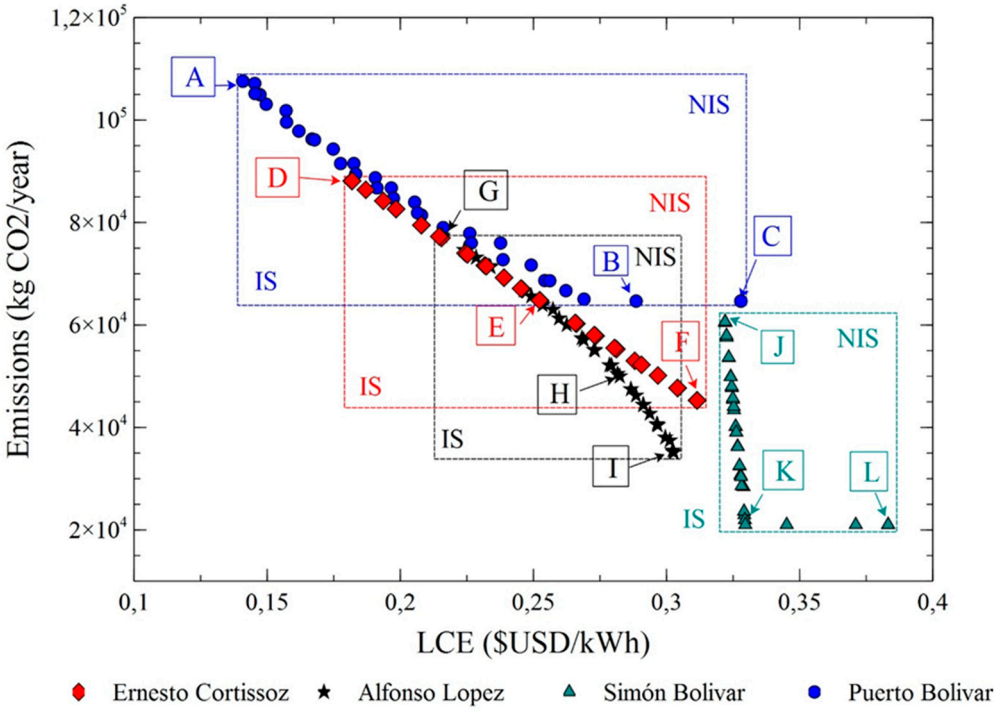

Figure 11. Pareto frontiers of LCE with CO_2 emissions for each location.

Figure 11 shows the areas of optimization composed by the zone of ideal solutions (IS) and the zone of non-ideal solutions (NIS). Also, shows high values of CO_2 emissions at the Puerto Bolivar, so much so that the optimized minimum value is greater than the maximum amount of CO_2 emissions by the system located at Simon Bolivar. Also, it is observed that the optimum values in the Ernesto Cortissoz and Alfonso Lopez systems are similar, therefore, your possible ideal solutions will be close to each other. The figure indicates that the system with the highest cost per kWh generated is the one located in Simon Bolivar, but it is also the system with the lowest CO_2 emissions.

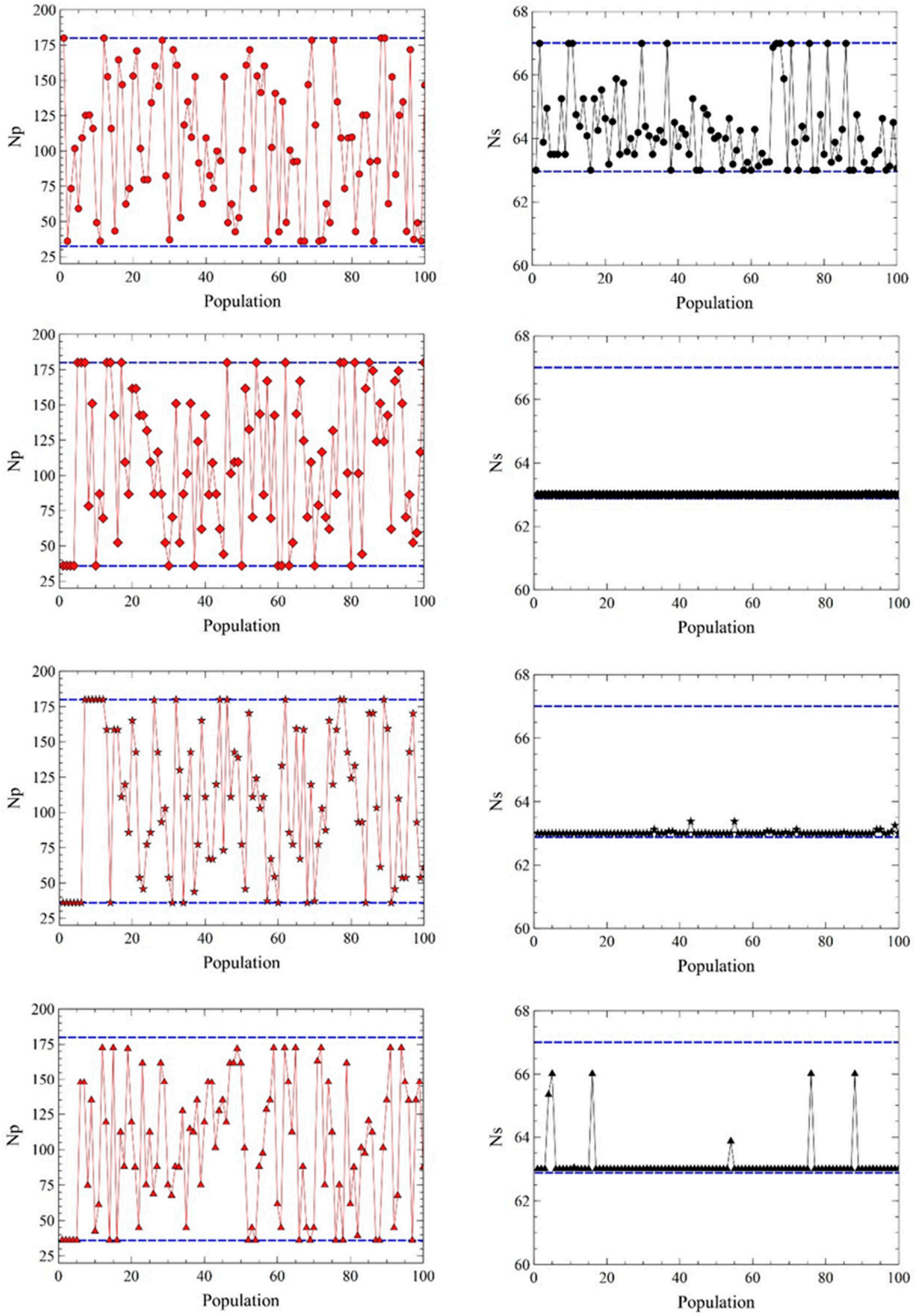

Figure 12. Dispersed distribution of decision criteria for LCE and CO_2 emissions with population at the Pareto frontier for each of the locations; a) C1, b) C2

Figure 12 presents the dispersed distributions of the design variables that evidence the evolution of their values during the optimization process for the Puerto Bolívar, Ernesto Cortissoz, Alfonso Lopez and Simon Bolívar locations, located from top to bottom, respectively. In other words, Figure 12a shows the evolution of the number of panels selected as the first selection criterion during optimization and, in addition to top-down represents the evolution in each of the locations; Figure

12b represents the same conditions for the second criterion that corresponds to the number of stacks. For Puerto Bolivar, the number of panels has a dispersed distribution centered, this indicates that its trend is not close to any of the limits of the variable. The second criterion if it has a tendency close to one of its limits, and that is that the evolution of the number of stacks tends to the upper limit of the domain during optimization, therefore suggests that this criterion puts at risk the minimization of both functions.

The second row refers to the location of Ernesto Cortissoz, here is shown an evolution of the number of panels very dispersed with a centered distribution and you can also see that there is no dispersion in the evolution of the number of stacks during optimization, taking the value of the lower limit. This suggests that the latter is the selection criterion that guarantees the solution closest to the ideal.

The evolution of Alfonso Lopez is similar to that described in Ernesto Cortissoz with respect to the number of panels. On the other side, during the distribution of the values of the number of stacks some have presented small dispersions that try to move away from the lower limit of the domain, they are not significant but even so they indicate a variation of the criteria of decision. Likewise, the locality of Simon Bolívar shows a distribution similar to the previous ones with respect to the number of panels; but it shows high dispersions in the evolution of the number of stacks, which suggests some compensations during the optimization.

The results indicate that these design variables are determinant to identify the critical points of the objective functions proposed for the optimization of the systems.

The optimization problem generates multiple possible solutions that correspond to optimal values limited by the design constraints of the system, as shown in Figure 11. For this reason, it is necessary to use a mathematical algorithm that identifies the point with the solution closest to the ideal [39]-[40]. In this article we present the Technique of Order Preference by Similarity with the Ideal Solution (TOPSIS) for the choice of the final solution. Its mathematical principle is based on the identification of the point with the shortest distance from the ideal positive solution and, to itself, with the longest distance from the ideal negative solution; conditions that are calculated by Equation 24

$$d_{ib} = \sqrt{\sum_{j=1}^{n} \left(t_{ij} - t_{bj}\right)^2}, \quad i = 1,2,\dots,m$$
$$d_{iw} = \sqrt{\sum_{j=1}^{n} \left(t_{ij} - t_{wj}\right)^2}, \quad i = 1,2,\dots,m \tag{24}$$

where d_{ib} and d_{iw} are the distances from the points to the ideal positive and negative solution, respectively; t_{ij} is the reference value of alternative i for objective j, t_{bj} and t_{wj} are the ideal and non-ideal values, respectively.

The relative proximity to the ideal solution (S_{iw}) is calculated using Equation 25

$$S_{iw} = {d_{iw}}/{(d_{iw} + d_{ib})} \qquad 0 \le S_{iw} \le 1 \tag{25}$$

where the best solution is the one whose S_{iw} is the closest to 1.

Figure 11 shows the twelve points that meet the optimization requirements, in addition, the intermediate points at each border correspond to the optimal values calculated with TOPSIS. Table 2 shows the values of the model parameters evaluated at each of the optimal points of the Pareto frontiers.

374 **Table 2.** Optimized values of parameters and objective functions.

	Parameters of design											
Units	N_p	N_s	n_{O_2}	n_{H_2}	P_{PV}	E_{wind}	E_{PEM}	E_{nu}	E_{net}	C_{tot}	LCE	Emissions
	-	-	mol	Mol	W	W	W	W	kWh	$USD	$USD/kWh	$kg/year$
Ref	36	65	0,0273	0,0273	13.184	52.446	14.757	7.388	769.306	208.657	0,2988	64.671,64
A	180	63	0,0273	0,0273	64.324	52.446	7.275	51.045	1534.544	195.051	**0,1408**	107.584,42
B	**36**	**64**	**0,0273**	**0,0273**	**13.184**	**52.446**	**14.757**	**7.388**	**769.306**	**208.657**	**0,2885**	**64.661,49**
C	36	67	0,0273	0,0273	13.184	52.446	14.757	7.388	769.306	208.657	0,3279	**64.661,47**
Ref	36	65	0,0734	0,0459	13.246	32.964	29.730	2.941	691.348	208.657	0,3325	45.179,31
D	180	63	0,0273	0,0273	64.623	32.964	7.138	31.726	1195.909	195.051	**0,1817**	88.119,16
E	**102**	**63**	**0,0273**	**0,0273**	**37.130**	**32.964**	**13.421**	**10.516**	**824.123**	**189.532**	**0,2525**	**64.738,88**
F	36	63	0,1501	0,0922	13.246	32.964	29.730	2.941	691.348	184.014	0,3114	**45.279,78**
Ref	36	65	0,1322	0,079	13.138	23.016	39.340	2.495	683.536	208.657	0,2988	64.671,64
G	180	63	0,0273	0,0273	64.101	23.016	6.461	20.579	1000.519	195.051	**0,2154**	77.455,43
H	**77**	**63**	**0,1091**	**0,1156**	**27.028**	**23.016**	**27.413**	**5.258**	**725.039**	**186.773**	**0,2866**	**47.475,15**
I	36	63	0,1322	0,079	13.138	23.016	39.340	2.495	683.536	184.014	0,3026	**35.141,09**
Ref	36	65	0,2102	0,1219	13.027	9.018	50.954	0	639.789	208.657	0,3593	21.022,60
J	172	63	0,0273	0,0273	60.749	9.018	7.280	4.049	710.762	242.767	**0,3220**	60.629,99
K	**39**	**63**	**0,2238**	**0.5678**	**14.102**	**9.018**	**49.878**	**0**	**639.789**	**184.014**	**0,3294**	**21.959,29**
L	36	66	0,1809	0,6725	13.027	9.018	50.954	0	639.789	221.424	0,3832	**21.026,78**

375

376 The multi-criteria decision technique indicated that points B, E, H and K are nearest to the ideal
377 solution, therefore, are considered the optimized values for the solution of the case studies.
378
379 **Table 3.** Multi-objective optimal solution.

Cases studies	Objective functions values		Criteria values	
	LCE ($USD/kWh)	Emissions (kg CO_2/year)	C1	C2
Puerto Bolívar	0,2885	64.661,49	36	64
Ernesto Cortissoz	0,2525	64.738,88	102	63
Alfonso Lopez	0,2866	47.475,15	77	63
Simon Bolívar	0,3294	21.959,29	39	63

380
381 Table 3 shows the optimal results of the multi-objective optimizations for each location. The
382 Ernesto Cortissoz airport represents a total cost of $189.532 USD and, in turn, the lowest costs for
383 power generation with a generating capacity of 824.123 kWh of which 10.516 W (11,2%) are not used.
384 This result is explained by the greater number of panels installed compared to other locations, due to
385 it increases the capacity of energy generation system. Also, this provides an increase in the amount
386 of emissions as a result of the process of generating solar energy. On the other hand, Puerto Bolivar
387 represents a total cost of $208.657 USD for the generation of 769.306 kWh of which 7.388 W (8,4%) of
388 energy is not used. Alfonso Lopez airport has a system with a generating capacity of 725.039 kWh of
389 which 5.258 W (6,35%) are not used, and the total cost of the system is $186.773 USD, while the system
390 operating in Simon bolivar airport has a cost of $184.014 USD and a generation capacity of 639.789
391 kWh fully usable which means a maximum use of production.
392

393 **5. Conclusions**

In the various countries where hybrid energy generation systems have been implemented and used, there have been positive results in the energy transition due to the advantages of renewable energy generation systems. In Colombia, specifically in the Caribbean region, there is an important renewable resource that, when complemented with electrochemical generation systems such as the cell in a hybrid system, presents results of great operational viability. When evaluating the performance of the system in the different places studied, a similar solar power profile was noted due to the proximity of these places in the Colombian Caribbean region.

As far as the generated wind power is concerned, there is a significant difference between the Puerto Bolivar station and the others, for which the implementation of a PEM is of great help in departments such as Magdalena, where the almost obligatory use of the PEM for the 200W demand is noted, however, In the case of the station located in La Guajira (Puerto Bolivar), the use of the PEM has no significant effect on the overall generation of the system, given that at this point the highest wind power values in the country are presented, implying a low load operation of the PEM cell type. The results of the wind energy generated show the stock of areas that can be estimated as important wind resources, such as Puerto Bolivar and Ernesto Cortissoz airport, places where the hybrid system would operate with the cell at low load.

The multivariate optimization analysis showed that at the Ernesto Cortissoz airport, although the highest total cost was obtained, the lowest costs were obtained for the generation of energy, however, there are greater quantities of CO_2 emissions due to the large number of solar panels used. By reducing the number of elements used in the different places studied, it was not guaranteed a much more environmentally friendly system, as is the case of Puerto Bolivar that used 1/3 part of solar panels in parallel and obtained emissions of kg CO_2 per year and energy costs similar to the airport Ernesto Cortissoz. On the other hand, at Simón Bolívar airport the optimization obtained the lowest emissions at a much higher energy cost because all the energy generated was consumed.

Author Contributions: All the authors of the present research contributed equally to conducting and writing this paper.

Funding: This research received no external funding.

Acknowledgments: Acknowledgments to Universidad del Atlántico, to the mechanical engineering program and Department of Energy of Universidad de la Costa.

Conflicts of Interest: The authors declare no conflict of interest.

Abbreviations

The following abbreviations are used in this manuscript:

COM	operating and maintenance cost
LCE	levelized cost energy
PEM	proton exchange membrane
PH	photogenerated
PID	proportional, integral and derivative
SHGEE	hybrid electric power generation system

Nomenclature

A_r	Flow area
C	Capacitance
CO_2	Oxygen concentration at the liquid-gas interface
E	Energy
F	Faraday Constant

h	Height
I	Electric current of the PEM cell
i	Bank interest rate
K	Boltzmann constant
Ki	Temperature coefficient of the short-circuit current
M	Molar flow
N	Number of component connected in the system
P	Pressure
q	Electron Charge
R	Universal gas constant
RE	Resistance
R_t	Thermal resistance
T	Operating temperature
U	Fuel speed
V	Wind speed
Vol	Volume
V	Voltage
Subscript	
0	reference state
A	Anode
ACT	Activation
E	electrolyze
INT	Internal
PV	Photovoltaic
S	Serial
SCR	short-circuit
T	Thermal
TOT	Total
Greek Symbol	
ρ	molar density of gases
ε_{CO_2}	CO_2 emissions for the PV systems
η_{act}	Overvoltage due to activation
η_c	Serial electrolyzed number
η_F	Faraday Efficiency
η_{H2}	Hydrogen molar flux produced
η_{ohmic}	Ohmic voltage
λ	Lighting of photovoltaic modules
$\propto$	roughness coefficient

References

[1] S. Ahmed, A. Mahmood, A. Hasan, G. A. S. Sidhu, and M. F. U. Butt. A comparative review of China, India and Pakistan renewable energy sectors and sharing opportunities. *Renew. Sustain. Energy Rev.*

2016,57,216–225.

[2] A. Sinha. Inequality of renewable energy generation across OECD countries: A note. *Renew. Sustain. Energy Rev.* **2017**,79,9–14.

[3] K. Kim, H. Park, and H. Kim. Real options analysis for renewable energy investment decisions in developing countries. *Renew. Sustain. Energy Rev.* **2017**,75,918–926.

[4] A. K. Shukla, K. Sudhakar, and P. Baredar. Renewable energy resources in South Asian countries: Challenges, policy and recommendations. *Resour. Technol.* **2017,**3,342–346.

[5] M. López-Losana. Análisis de la producción científica sobre patología dual en prisión. **2013,**218.

[6] L. M. Romo Fernández, V. P. Guerrero Bote, and F. Moya Anegón. Análisis de la producción científica española en energías renovables, sostenibilidad y medio ambiente (Scopus, 2003-2009) en el contexto mundial. *Investig. Bibl. Arch. Bibl. e Inf.* **2013**,27,125–151.

[7] L. M. Romo-Fernández, C. López-Pujalte, V. P. Guerrero Bote, and F. Moya-Anegón. Analysis of Europe's scientific production on renewable energies. *Renew. Energy.* **2011**,36,2529–2537.

[8] A. Holma et al. Environmental impacts and risks of the national renewable energy targets – A review and a qualitative case study from Finland. *Renew. Sustain. Energy Rev.* **2018,**82,1433–1441.

[9] Congreso de Colombia. Ley N° 1715 del 13 de mayo de 2014. *Upme* **2014**,26.

[10] S. A. Abbasi, Tabassum-Abbasi, and T. Abbasi. Impact of wind-energy generation on climate: A rising spectre. *Renew. Sustain. Energy Rev.* **2016**,59,1591–1598.

[11] N. Kannan and D. Vakeesan. Solar energy for future world: - A review. *Renew. Sustain. Energy Rev.* **2016**,62,1092–1105.

[12] M. R. Islam, S. Mekhilef, and R. Saidur. Progress and recent trends of wind energy technology. *Renew. Sustain. Energy Rev* **2013**,21,456–468.

[13] Procolombia. Electric Power in Colombia. *Power Generation* - 2015. **2015**,23

[14] M. Y. Recalde, D. H. Bouille, and L. O. Girardin. LIMITACIO PARA EL DESARROLLO DE ENERGÍAS RENOVABLES EN ARGENTINA. *Probl. Desarro.* **2015**,46,89–115.

[15] F. B. Budes, Y. C. Escorcia, and G. V. Ochoa. Optimization of a Biomass , solar and fuel cell Hybrid energy systems for a specific energy load using Homer Pro software ®. *Inter. Journal of ChemTech Res.* **2018**,11,335–340.

[16] M. Sikka, T. F. Thornton, and R. Worl. Sustainable Biomass Energy and Indigenous Cultural Models of Well-being in an Alaska Forest Ecosystem. *Ecol. Soc*. **2013**,18,531–543.

[17] A. Vides-Prado et al. Techno-economic feasibility analysis of photovoltaic systems in remote areas for indigenous communities in the Colombian Guajira. *Renew. Sustain. Energy Rev*. **2018**, 82,4245–4255.

[18] Sistema de informacion Eléctrico Colombiano (SIEL) **2018**. [Online]. Available: http://www.siel.gov.co/Inicio/CoberturadelSistemaIntercontecadoNacional/ConsultasEstadisticas/tabid/81/Default.aspx. [Accessed: 22-Feb-2018].

[19] M. Mikati, M. Santos, and C. Armenta. Modelado y Simulación de un Sistema Conjunto de Energía Solar y Eólica para Analizar su Dependencia de la Red Eléctrica. *Rev. Iberoam. Automática e Informática Ind. RIAI* **2012**,9,267–281.

[20] C. Bordons, F. García-Torres, and L. Valverde. Gestión Óptima de la Energía en Microrredes con Generación Renovable. *Rev. Iberoam. Automática e Informática Ind. RIAI* **2015**,12,117–132.

[21] A. López, J. A. Somolinos, and L. R. Núñez. Modelado Energético de Convertidores Primarios para el Aprovechamiento de las Energías Renovables Marinas. *Rev. Iberoam. Automática e Informática Ind. RIAI* **2014**,11,224–235.

[22] C. L. de A. Dias, D. A. Castelo Branco, M. C. Arouca, and L. F. Loureiro Legey. Performance estimation of photovoltaic technologies in Brazil. *Renew. Energy* **2017**,114,367–375.

[23] D. Abbes, A. Martinez, and G. Champenois. Life cycle cost, embodied energy and loss of power supply probability for the optimal design of hybrid power systems. *Math. Comput. Simul*. **2014**,98,46–62.

[24] B. Parida, S. Iniyan, and R. Goic. A review of solar photovoltaic technologies. *Renew. Sustain. Energy Rev.* **2011**,15,1625–1636.

[25] G. Chicco and P. Mancarella. A unified model for energy and environmental performance assessment of natural gas-fueled poly-generation systems. *Energy Convers. Manag*. **2008**,49,2069–2077.

[26] Y. Cancino-Solórzano and J. Xiberta-Bernat. Statistical analysis of wind power in the region of Veracruz (Mexico). *Renew. Energy* **2009**,34,1628–1634.

[27] O. del C. Colombiano. Región Caribe Colombiana **2015**. [Online]. Available: http://www.ocaribe.org/region-caribe.

[28] N. Pandiarajan, R. Ramaprabha, and R. Muthu. Application of circuit model for photovoltaic energy conversion system. *Int. J. Photoenergy* **2012**.

[29] G. Valencia Ochoa, C. Blanco, C. Martinez, and E. Ramos. Fuzzy Adaptive Control Applied to a Hybrid Electric-Power Generation System (HEPGS). *Indian J. Sci. Technol*. **2017**,10,1–9.

[30] S. Esmaeili and M. Shafiee. Simulation of Dynamic Response of Small Wind-Photovoltaic-Fuel Cell Hybrid Energy System. *Scientific Research* **2012**,194–203.

[31] G. N. D. Sens S. Anaerobic tratment of real textile wastewater with a fluidized bed reactor. *Water Res*. 2003,37.

[32] J. Gabriel García Clúa, R. Julián Mantz, and H. De Battista. Hybrid control of a photovoltaic-hydrogen energy system. *Int. J. Hydrogen Energy* 2008,33,3455–3459.

[33] Krismadinata, N. A. Rahim, H. W. Ping, and J. Selvaraj. Photovoltaic Module Modeling using Simulink/Matlab. *Procedia Environ. Sci*. **2013**,17,537–546.

[34] J. J. Hwang, L. K. Lai, W. Wu, and W. R. Chang. Dynamic modeling of a photovoltaic hydrogen fuel cell hybrid system. *Int. J. Hydrogen Energy* **2009**,34,9531–9542.

[35] R. V. Padilla, G. Demirkaya, D. Y. Goswami, E. Stefanakos, and M. M. Rahman. Heat transfer analysis of parabolic trough solar receiver. *Appl. Energy* **2011**,88,5097–5110.

[36] G. Valencia Ochoa, M. Vanegas Chamorro, and J. Polo Jiménez. Análisis estadístico de la velocidad y dirección del viento en la región caribe colombiana con énfasis en la Guajira. **2016**.